Mechanisms of reentry arrhythmia termination with ephaptic coupling and gap junctional coupling

Ning Wei[1, a)] and Joyce Lin[2, b)]
[1)]*Department of Mathematics, Purdue University, West Lafayette, IN 47907, USA*
[2)]*Mathematics Department, California Polytechnic State University, 1 Grand Ave, San Luis Obispo, CA 93407*

(Dated: 29 May 2025)

Cardiac cells communicate electrically to coordinate heart contractions and pump blood. Gap junctions in the intercalated discs (ID) between myocytes form low-resistance pathways that facilitate electrical propagation. Traditionally, gap junctional coupling is considered the primary mechanism for cell communication, but experimental studies show that conduction can persist even with impaired gap junctions. For example, in gap junction-deficient rats, the heart still shows slow, discontinuous signal propagation, suggesting the existence of other communication mechanisms. One such mechanism is ephaptic coupling (EpC), an electrical field effect in the ID that maintains conduction even in the absence of gap junctions. EpC has been explored experimentally and numerically, especially in altered ID under normal and diseased conditions. However, a lack of direct evidence emphasizes the need to study its physiological role in the heart. Some research indicates that EpC can increase conduction velocity and reduce conduction failure, but its effects on cardiac arrhythmias are not well understood. Our study focuses on reentry arrhythmia, where rapid, irregular heartbeats can lead to cardiac arrest. Previous modeling work suggests that strong EpC can terminate reentry in ischemic hearts, though the mechanism remains unclear. We aim to investigate the mechanisms underlying reentry termination across different levels of EpC and gap junctional coupling using a two-dimensional discrete bidomain model with EpC. Our results identify two mechanisms: (1) strong EpC terminates reentry through self-attenuation and (2) moderate EpC terminates reentry through self-collision, influenced by increased conduction velocity and anisotropy. A boundary where termination does not occur is also observed.

Cardiac cells synchronize contractions to pump blood through electrical communication. Gap junctions in the intercalated discs (IDs) between myocytes provide low-resistance pathways for impulse propagation[1–4]. Although gap junctional coupling has been seen as the primary mechanism[5], experimental studies show that conduction can still occur even with impaired junctions[6,7]. For instance, gap junction-deficient rats exhibit slow and discontinuous signal propagation[6], suggesting alternative mechanisms like ephaptic coupling (EpC), which involves electrical fields in the narrow clefts between myocytes. Although EpC has been studied experimentally, direct evidence is still lacking, which has led to investigations into its physiological role in the heart. Some research indicates that EpC can sustain conduction when gap junctional coupling is compromised[8,9]. Our study focuses on reentry arrhythmia, where electrical impulses repeatedly activate heart tissue, potentially leading to cardiac arrest. Our previous work suggests that EpC can terminate reentry[10], but the mechanism is unclear. We investigated reentry termination at varying levels of EpC and gap junctional coupling, finding that strong EpC leads to self-attenuation, while moderate EpC results in self-collision due to increased anisotropy and speed of conduction. We also identified a boundary between these regimes, often showing no termination. Our mechanistic understanding of EpC will greatly aid in elucidating its nature.

[a)]Electronic mail: wei307@purdue.edu
[b)]Electronic mail: jlin46@calpoly.edu

I. INTRODUCTION

Cardiac cells coordinate the contraction of the heart muscles to pump blood through electrical communication. Gap junctions, situated in the intercalated disc (ID) between myocytes, serve as low-resistance pathways facilitating electrical connections among cardiac cells, thereby mediating the propagation of electrical impulses[1–4]. It is widely acknowledged that gap junctional coupling is the primary mechanism for cell communication[5]. However, experimental observations have raised questions about whether conduction can be maintained in the absence of gap junctions[6,7]. For example, in[7], intercellular conductance in pairs of gap junction-deficient adult rat myocytes was significantly reduced from 588 nS to 10 nS. However, the resulting impulse propagation was only reduced by 50%, suggesting the existence of alternative mechanisms for cell communication in the heart.

Ephaptic coupling (EpC) is an alternative mechanism of cardiac conduction suggested to explain the propagation of electrical activity in the heart when gap junctions are compromised. In the presence of EpC, cardiac conduction is believed to be maintained through the electrical fields in the narrow ID between adjacent myocytes[8,9]. EpC has been the subject of continuous experimental[11–14] and numerical[10,14–21] investigations, and alterations in the ID have been explored under both normal[11,14] and various diseased[12,13,22] conditions. However, direct experimental evidence — empirical data that clearly demonstrates EpC as a distinct and measurable phenomenon, separate from other mechanisms like gap junctional conduction—remains lacking. Consequently, attempts have been made to indirectly demonstrate the presence of EpC by exploring its physiological role in the heart under different

conditions. For instance, in[15,17–20,23–27], the authors showed that EpC can help maintain cardiac conduction and mitigate conduction block when gap junctional coupling is impaired. Despite this significant progress in research highlighting the impact of EpC on cardiac conduction, the implications of EpC on cardiac arrhythmias remain complex and have not been fully explored.

Here, we focus on reentry arrhythmia, a type of abnormal heart rhythm where the electrical impulses that control the heartbeat follow a circular path, repeatedly activating the heart tissue. This can lead to rapid and irregular heartbeats, which can cause cardiac arrest and sudden death. In[10], we observed only one instance of reentry termination during myocardial ischemia when EpC is very strong. The mechanisms of termination and the various ways it can occur, all of which are equally important, were not discussed in that paper. Moreover, myocardial ischemia introduces more complexity, exploring the mechanism is nearly impossible. Simpler conditions are necessary to understand the mechanism. Therefore, in this study, we aim to explore the effects of varying levels of EpC and gap junctional coupling, excluding ischemia, to gain a clearer understanding of the mechanisms underlying reentry termination. Our findings indicate two distinct scenarios for terminating reentry. Firstly, when EpC is sufficiently robust, reentry is terminated through self-attenuation. Furthermore, with moderate EpC, reentry is terminated through self-collision, driven by increased conduction velocity and anisotropy between the longitudinal and transverse directions. Moreover, a distinct boundary between these two regimes emerges in which no termination is exhibited.

II. MATERIALS AND METHODS

A. Model overview

We used our previously developed two-dimensional (2D) discrete bidomain model with EpC[10,19,20] to simulate cardiac conduction, which highly relies on the presence of junctional cleft space between adjacent cells. In this model, each cell is represented as a cylinder, and the cells are connected through gap junctions to form an $M \times N$ rectangular lattice. At each lattice point (i, j), we defined both the intracellular potential, $\phi_i^{(i,j)}$, and the extracellular potential, $\phi_e^{(i,j)}$. The junctional cleft lies between adjacent cells (i, j) and $(i, j+1)$, and we introduced a cleft potential, $\phi_c^{(i,j+\frac{1}{2})}$, at the position $(i, j+\frac{1}{2})$. The space adjacent to the cleft, which lies in the extracellular region, is referred to as the extracellular-cleft space, and the potential in this space is denoted by $\phi_{ec}^{(i,j+\frac{1}{2})}$.

The top panel of Fig. 1 illustrates the lattice view of the model, while the bottom panel presents a circuit diagram for two adjacent cells coupled through the shared cleft space and end-to-end gap junctions (GJ_{end}). However, side-to-side gap junctions (GJ_{side}) and the resistive connection (R_{ee}) between extracellular spaces in the transverse direction are not shown here. The cleft space is modeled as a narrow compartment with resistive connections (R_c) to the extracellular-cleft space, while resistive connections between the extracellular and extracellular-cleft spaces are represented by R_{ec}. The intracellular and extracellular spaces of each cell are separated by the cell side membrane, and the intracellular and cleft spaces are separated by the cell end membrane. The side and end membranes function independently, permitting flow of ionic and capacitive currents. To reduce computational complexity, we assumed that the intracellular and extracellular spaces of each cell are isopotential.

B. Modeling EpC

EpC highly relies on the presence of a cleft space between the ends of adjacent cells. This cleft space communicates with the end membranes of neighboring cells and the extracellular space independently. To model EpC, we derived an equation for the cleft space based on the current balance principles, considering the equilibrium of capacitive and ionic currents across two adjacent end membranes connected through a shared cleft potential, as well as the resistive currents between the cleft and the extracellular space, represented by R_c. The following equation illustrates this balance:

$$-A_{\text{end}}C_m\frac{\partial(\phi_i^{(i,j)}-\phi_{\text{c}}^{(i,j+\frac{1}{2})})}{\partial t}-A_{\text{end}}C_m\frac{\partial(\phi_i^{(i,j+1)}-\phi_{\text{c}}^{(i,j+\frac{1}{2})})}{\partial t}-I_{\text{end}}+\frac{\phi_c^{(i,j+\frac{1}{2})}-\phi_{ec}^{(i,j+\frac{1}{2})}}{R_c}=0. \tag{1}$$

R_c is inversely proportional to the cleft width (d_{cleft}), with the relevant formulas available in[20,24]. We selected d_{cleft} values ranging from 8 nm to 50 nm[10,19,20] to represent different levels of EpC. Notably, a smaller d_{cleft} corresponds to higher R_c, indicating a stronger EpC effect. Specifically, strong EpC is defined when $d_{\text{cleft}} \leq 8$ nm, medium EpC corresponds to d_{cleft} values between 10 nm and 20 nm, and weak EpC is characterized by d_{cleft} values greater than or equal to 20 nm. A d_{cleft} of 115 nm indicates minimal EpC influence.

The model equations were derived based on the current balance principles for the intracellular, extracellular, cleft, and extracellular-cleft spaces. Specifically, the current balance represents the equilibrium between capacitive currents, ionic currents, and resistive currents across the different domains. The detailed equations are provided in Eqs. (2.1) to (2.4) of our previous publication[20], and all parameters are listed in Table 1 of Ref.[20].

C. Membrane dynamics

To represent the dynamics of excitable cells in normal tissue, we employed the Luo-Rudy dynamic model of 2007 (LRd2007), which is specific to guinea pig ventricular tissue[28]. Furthermore, in our 2D model, the fast sodium (INa) channels are localized at the end membrane, as observed in experimental studies[29–31]. The localization of INa channels

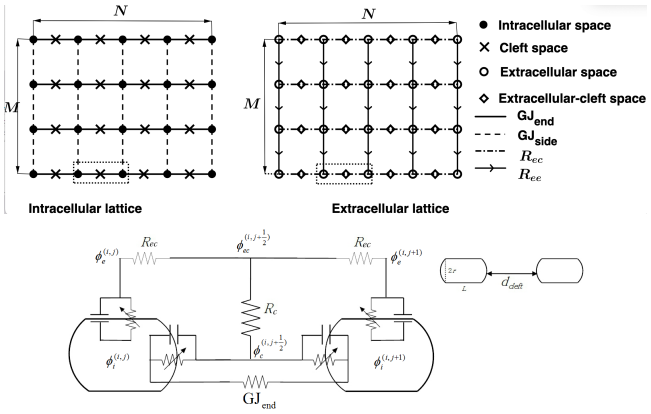

FIG. 1. **2D bidomain model with EpC.** Lattice representation of the model (top) and circuit diagram (bottom) for two adjacent cells coupled via a shared cleft[10,19,20].

was achieved by redistributing the channels across the end membrane, while keeping the total number of ionic channels or conductance constant. Other ionic channels are uniformly distributed across both the side and end membranes, with the channels and their corresponding gating variables functioning independently on each membrane.

D. Numerical scheme and pacing protocol

To solve a system of ordinary algebraic equations (Eqs. (2.1) to (2.4) in[20]), we employed a time-splitting method to independently update the potential, ionic concentration, and gating variables of the ion channels. Specifically, the linear components of the system were addressed using the backward Euler method, while the nonlinear components (e.g., ionic currents and dynamics) were initially linearized and then handled using the backward Euler method. The system was solved using a direct method (backslash operator in Matlab).

We conducted numerical simulations on a lattice consisting of $M \times N$ cells, where $M = N = 550$, employing a time step of 0.01 ms. Initially, all gating variables, ionic concentrations, and potentials were set to steady state. We first implemented an S1-S2 cross-field stimulation protocol to induce reentry in the near-absence of EpC across different levels of gap junctions, which is a standard method to induce reentrant arrhythmias in cardiac tissue in silico[32–35]. Note that perturbing the steady states has a minimal effect on reentry formation when EpC is nearly absent. To ensure that the effects we observed were not influenced by initial conditions or pacing protocols, we used the generated reentry at each level of gap junctional coupling as the initial condition and thereafter incorporated EpC to examine its impact on reentry termination.

Activation was monitored by plotting V_m (side transmembrane potential) across the 2D lattice. The wavefront of typical action potential propagation was characterized as the spatial point where V_m surpasses -30 mV, coupled with a positive temporal derivative $\left(\frac{\partial V_m}{\partial t} > 0\right)$. This threshold served as a criterion to differentiate normal action potential from small-amplitude action potential (SAP)[19,20]. SAP, as defined in[20], represents a novel form of action potential capable of propagating within cardiac tissue despite its diminished amplitude (maximum $V_m = -40$ mV).

III. RESULTS

In this section, we aim to explore the mechanisms underlying reentry termination at various levels of EpC and gap junction coupling. Fig. 2 shows snapshots at different time points—30 ms, 100 ms, 200 ms, and 300 ms—during a sustained reentry, when EpC is nearly absent ($d_{\text{cleft}} = 115$ nm) and gap junction coupling is at 100%.

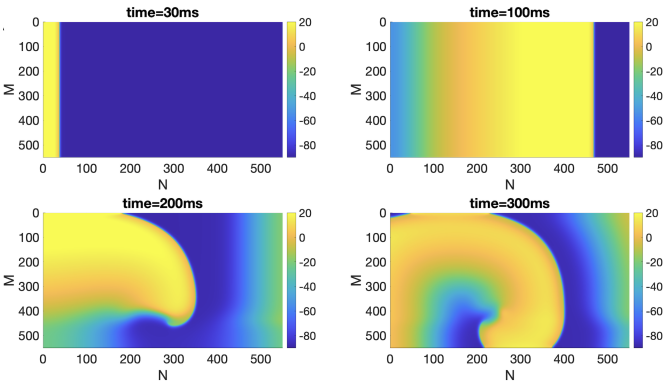

FIG. 2. **Sustained reentry with nearly absent EpC**. Snapshots of V_m at 30 ms, 100 ms, 200 ms, and 300 ms for $d_{\text{cleft}} = 115$ nm and 100% gap junction coupling.

As EpC increases due to a decrease in d_{cleft}, resistance to ion flow rises, impacting the conduction dynamics and stability of established reentrant circuits. Specifically, a reduction in d_{cleft} can prolong the refractory period and cause conduction block, disrupting the circular pathway essential for sustained reentry. As a result, two distinct types of termination emerge.

A sudden reduction to an extremely small d_{cleft} can lead to the first type of reentry termination, characterized by an immediate drop in V_m due to self-attenuation. Fig. 3 shows an example of reentry that terminates immediately due to self-attenuation when $d_{\text{cleft}} = 8$ nm and gap junctional coupling is 100%. This self-attenuation arises from the fast inactivation of INa channels, as shown in Fig. 4. The rapid inactivation of the m gate, essential for impulse propagation, is influenced by the increased resistance between the cleft space and the bulk extracellular space. As a result, sufficiently strong EpC can slow down conduction and lengthen the refractory period, ultimately leading to the rapid termination of reentry.

In Fig. 4, we showed the corresponding time profiles of the activation gate m of INa when reentry is terminated, as depicted in Fig. 3. We observed that the m gate drops to 0 within 50 ms when $d_{\text{cleft}} = 8$ nm (red). In contrast, when the cleft expands to 115 nm (green), the m gate activation decreases to 0 and then recovers to 1 within 20 ms.

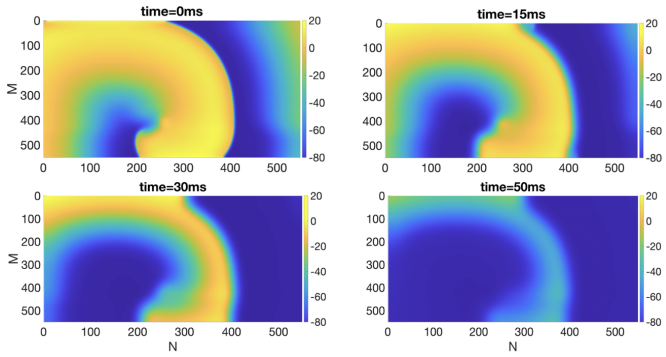

FIG. 3. **Reentry termination due to self attenuation.** Snapshots of V_m at 0 ms, 15 ms, 30 ms, and 50 ms showing reentry termination due to self-attenuation at $d_{\text{cleft}} = 8$ nm and 100% gap junctional coupling.

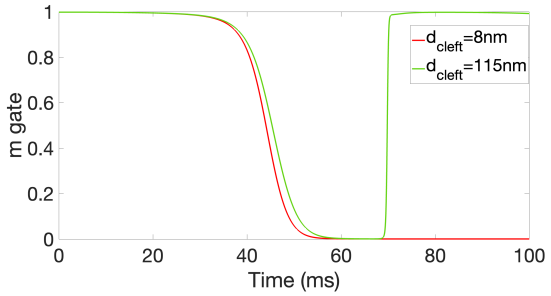

FIG. 4. **Temporal profiles of the m gate during reentry termination caused by self attenuation.** The time profiles of the m-gate are shown for d_{cleft} values of 8 nm (red) and 115 nm (green) with 100% gap junction coupling.

The second type of reentry termination involves self-attenuation combined with collision when d_{cleft} is at a medium level, where the action potential collides with itself multiple times before eventually terminating. Fig. 5 illustrates an example of reentry termination due to self-collision when $d_{\text{cleft}} = 12$ nm and gap junctional coupling is 100%, by showing snapshots of V_m before and during the self-collision. As shown in Fig. 5, reentry terminates after several cycles of collision, with termination occurring around 450 ms, which is approximately 10 times longer than self-attenuation. When EpC is at a moderate level, the altered conduction properties can lead to delays or blocks in impulse propagation, disrupting the circular pathway necessary for sustained reentry. Although the reentrant circuit can still trigger depolarization, it encounters tissue that has already been activated and is in a refractory state, resulting in a longer persistence of activity compared to self-attenuation.

In order to test whether the pattern of reentry termination dependent on d_{cleft} is consistent across different levels of gap junctional coupling, we presented Fig. 6, which summarizes two different types of termination at varying levels of EpC and gap junctional coupling. Data points are marked to indicate whether termination occurred due to self-attenuation (squares) or a combination of collision and self-attenuation (triangles), with diamonds representing cases where no termination occurred.

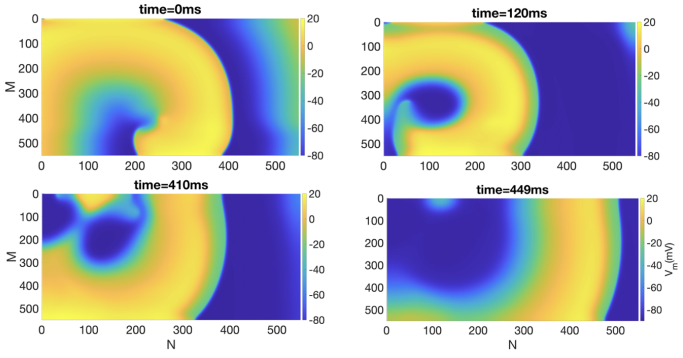

FIG. 5. **Reentry termination due to self collision.** Snapshots of V_m at 0 ms, 120 ms, 410 ms, and 449 ms showing reentry termination due to self-attenuation at $d_{\text{cleft}} = 12$ nm and 100% gap junctional coupling.

As indicated Fig. 6, we observed that d_{cleft} plays a more significant role than gap junctional coupling in determining the termination mechanism. A narrower cleft, regardless of gap junctional coupling, leads to self-attenuation, while a wider cleft triggers self-collision. Notably, between these two regimes, there is a distinct boundary that separates these two mechanisms of reentry termination, where no termination occurs. Within this boundary, impulses may enter a fragile state where neither self-collision nor self-attenuation occurs efficiently due to the complex interaction between sodium channel availability and the refractory period of surrounding myocardial cells. This results in a precarious stability, where reentrant activity may oscillate, potentially giving rise to abnormal arrhythmic patterns without a clear termination.

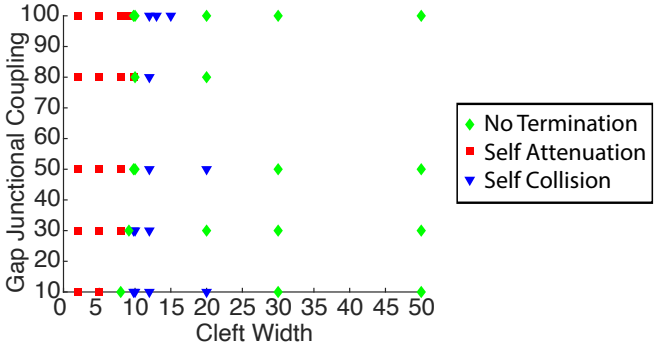

FIG. 6. **Summary of Termination Mechanism.** Simulations that resulted in self attentuation (squares), self attenuation and collision (triangles), or no termination (diamonds) are shown as a function of cleft width and gap junctional coupling.

To identify the potential factors contributing to each termination mechanism, we relocated the INa channels to the side membrane of each cell, instead of positioning them at the cleft. As a result, the reentry arrhythmia no longer terminates. This suggests that the termination process depends on the preferential placement of INa channels at the clefts, regardless of the underlying mechanism. Additionally, we in-

vestigated the effect of extracellular resistance, R_{ee} and R_{ec}, on reentry termination. We reduced R_{ee} and R_{ec} to nearly zero while maintaining the resistance R_c between the cleft and the extracellular space. Fig. 7 illustrates the termination types with extracellular resistance near zero and gap junctional coupling at 100% (left) and 10% (right). As shown in Fig. 7, we observed that with 100% gap junctional coupling, as extracellular resistance approaches zero, termination caused by self-attenuation occurs across a wider range of cleft sizes, while the occurrence of termination failures decreases. In contrast, at 10% gap junctional coupling, the type of termination is unaffected by extracellular resistance.

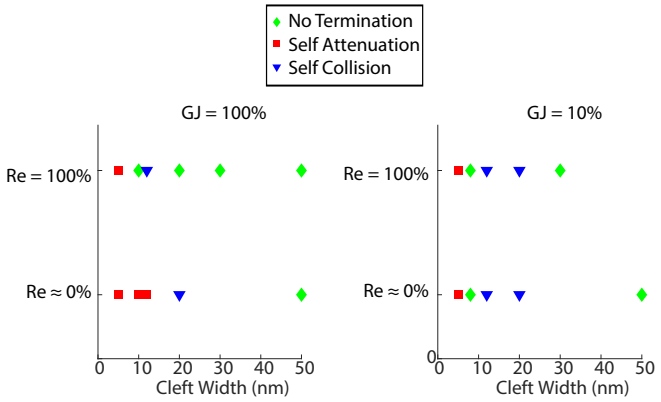

FIG. 7. **Reentry Termination Types Across Varying Extracellular Resistance and Gap Junctional Coupling.** 100% gap junctional coupling (left) with data for normal and nearly zero extracellular resistance; 10% gap junctional coupling (right) with the same variation in extracellular resistance.

Fig. 8 depicts the conduction velocities in both the transverse and longitudinal directions, along with the corresponding anisotropy ratio for several cases shown in Fig. 7. As the action potential wavefront generally propagates in a circular motion, the conduction velocities in the longitudinal and transverse directions vary depending on the wavefront's position within its circular trajectory. We calculated the transverse conduction (instantaneous velocity) at a specific point when the wavefront is moving solely in the transverse direction (up or down) and the longitudinal velocity when it is moving in the longitudinal direction (left or right). It is important to note that we do not measure velocities at all instances when the wavefront is moving exclusively in one direction; instead, we report a single representative value for each simulation, taken around the midpoint when the wavefronts are colliding with each other.

In the left panel of Fig. 8, it is seen that under 100% gap junctional coupling and extracellular resistance (black), conduction velocities (top) increase monotonically with cleft width. However, anisotropy (bottom) reaches a peak near the transition points where self-collision is identified as the cause of termination. When extracellular resistance approaches zero (blue), the behaviors remain qualitatively similar, with anisotropy peaking around the point where self-collision terminations occur.

In the right panel of Fig. 8, an overall decrease in conduction velocity (top) is observed when gap junctional coupling is set to 10%. With normal extracellular resistance, a biphasic effect is seen in the conduction velocities (black). However, when extracellular resistance is near zero, this biphasic effect disappears (blue), consistent with our previous observations[16]. Additionally, the anisotropy ratio still peaks at the points where termination types transition.

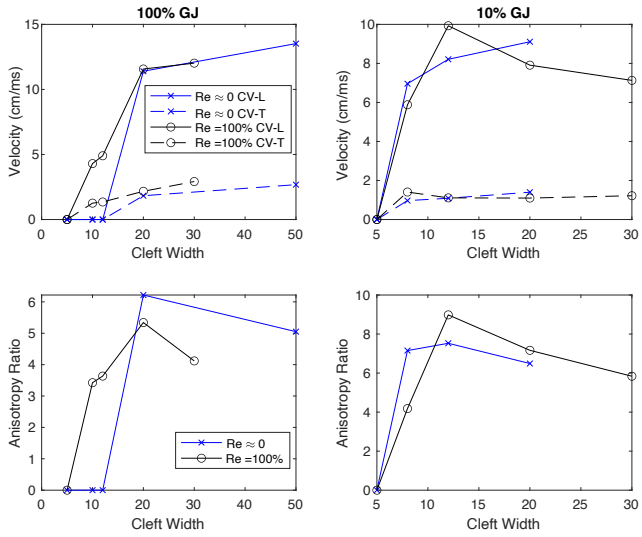

FIG. 8. **Conduction Velocities and Anisotropy Ratios for Varying Cleft Width, Gap Junctional Coupling, and Extracellular Resistance.** Top row: Conduction velocities for 100% (left) and 10% (right) gap junctional coupling in the longitudinal (solid) and transverse (dashed) directions, with extracellular resistance at 100% (black) and near zero (blue). Bottom row: Anisotropy ratios for 100% (left) and 10% (right) gap junctional coupling, with extracellular resistance at 100% (black) and near zero (blue).

The analysis of data from Figs. 7 and 8 shows that self-collision occurs when conduction velocities in both longitudinal and transverse directions are high, and anisotropy ratios are elevated. A rapidly traveling action potential will collide with itself before the excited tissue has time to return to equilibrium. Additionally, in cases of self-attenuation, propagation dissipates immediately, with velocities and anisotropy ratios reaching zero.

When exploring the complex mechanism of reentry termination, the interaction between self-attenuation and anisotropy plays a crucial role. Specifically, when $d_{\text{cleft}} \leqslant$ 8 nm, self-attenuation is the dominant mechanism for reentry termination. As d_{cleft} increases to approximately 9.8 nm – 10 nm, the anisotropy ratio also increases; however, the effect of self-attenuation decreases, resulting in a balance between the two effects, where no termination occurs. When the d_{cleft} increases further to around 12 nm – 20 nm, the self collisions, driven by the high anisotropy ratio, lead to termination. However, as the cleft width continues to grow ($d_{\text{cleft}} \geqslant 30$ nm), the influence of self-attenuation and collisions diminishes, resulting in the absence of termination.

IV. DISCUSSION

In this study, we investigated the process of reentry termination under varying levels of EpC and gap junctional coupling. Our findings reveal two distinct mechanisms for terminating reentry. First, when cleft width is small, reentry is terminated through self-attenuation. In contrast, with moderate cleft width, reentry is terminated by self-collision, driven by increased anisotropy (the ratio of conduction velocity between the longitudinal and transverse directions) along with higher conduction speeds. Additionally, a clear boundary between these two mechanisms emerges, where reentry termination is not observed.

EpC significantly contributes to preserving action potential propagation[8–21] by enhancing conduction velocity and minimizing the conduction block, it has also been shown that EpC can terminate reentry under ischemic conditions[10]. However, the precise mechanisms governing reentry termination remain unclear. Therefore, our current study holds significance in exploring the role of EpC and its corresponding mechanisms on arrhythmogenesis in the heart. EpC is an intriguing phenomenon, crucial yet challenging to study directly through experimental means due to the nanoscale ID, presumed to be the origin of EpC. Nonetheless, gaining a mechanistic understanding of EpC will be immensely valuable in elucidating its nature.

We induced reentry using the cross-field S1-S2 pacing protocol. This method of generating reentry parallels the effects of various triggers and sustainers, which has been extensively studied to understand cardiac electrophysiological properties, contributing to the elucidation of mechanisms underlying various arrhythmias[36,37]. The S1-S2 pacing protocol is not only integral in experimental research but also holds clinical relevance in arrhythmia assessment and management strategies. By utilizing this pacing technique, clinicians can explore the vulnerability of cardiac tissues to reentrant arrhythmias, aiding in the development of targeted therapeutic approaches for patients with arrhythmogenic potential[35,38].

The ongoing investigation into the mechanism of EpC also unveils unknown phenomena. Specifically, the boundary delineating these two mechanisms of reentry termination is intriguing yet unclear. We intend to conduct a bifurcation analysis to delve deeper into the detailed mechanisms underlying this boundary. We believe that comprehending the boundary that distinguishes these two distinct regimes in terminating reentry will, in turn, aid in understanding the mechanism of termination in the presence of EpC.

However, our current study also presents some limitations. Specifically, we have overlooked the detailed cell geometry, the microdomain effect of the extracellular space, and the complex geometry of the ID, all of which could potentially contribute to reentry termination. Nonetheless, providing a detailed description of these factors would pose a significant challenge to our study, as it would substantially increase computational costs. Our current findings suggest that these factors may not be critical in reentry termination. However, investigating the individual impact of each on reentry termination will be the focus of our future work.

V. ACKNOWLEDGMENTS

This study is supported by NSF grants DMS-2327184 and DMS-2152115 awarded to Ning Wei, as well as the Simons Collaboration Grant for Mathematicians 855881 to Ning Wei.

VI. AUTHOR CONTRIBUTIONS

Ning Wei designed the numerical experiments and ran the numerical simulation; Ning Wei and Joyce Lin analyzed the results; Ning Wei and Joyce Lin wrote and edited the manuscript.

VII. CONFLICT OF INTEREST

The authors declare no competing interests.

VIII. DATA AVAILABILITY STATEMENTS

The data that support the findings of this study are available within the article.

IX. REFERENCE

[1]R. M. Shaw and Y. Rudy, "Ionic mechanisms of propagation in cardiac tissue: roles of the sodium and l-type calcium currents during reduced excitability and decreased gap junction coupling," Circulation research **81**, 727–741 (1997).

[2]D. Vaidya, H. S. Tamaddon, C. W. Lo, S. M. Taffet, M. Delmar, G. E. Morley, and J. Jalife, "Null mutation of connexin43 causes slow propagation of ventricular activation in the late stages of mouse embryonic development," Circulation research **88**, 1196–1202 (2001).

[3]P. Beauchamp, C. Choby, T. Desplantez, K. de Peyer, K. Green, K. A. Yamada, R. Weingart, J. E. Saffitz, and A. G. Kléber, "Electrical propagation in synthetic ventricular myocyte strands from germline connexin43 knockout mice," Circulation research **95**, 170–178 (2004).

[4]P. Beauchamp, T. Desplantez, M. L. McCain, W. Li, A. Asimaki, G. Rigoli, K. K. Parker, J. E. Saffitz, and A. G. Kleber, "Electrical coupling and propagation in engineered ventricular myocardium with heterogeneous expression of connexin43," Circulation research **110**, 1445–1453 (2012).

[5]S. Rohr, "Role of gap junctions in the propagation of the cardiac action potential," Cardiovascular research **62**, 309–322 (2004).

[6]S. B. Danik, F. Liu, J. Zhang, H. J. Suk, G. E. Morley, G. I. Fishman, and D. E. Gutstein, "Modulation of cardiac gap junction expression and arrhythmic susceptibility," Circulation research **95**, 1035–1041 (2004).

[7]J.-A. Yao, D. E. Gutstein, F. Liu, G. I. Fishman, and A. L. Wit, "Cell coupling between ventricular myocyte pairs from connexin43-deficient murine hearts," Circulation research **93**, 736–743 (2003).

[8]N. Sperelakis, "An electric field mechanism for transmission of excitation between myocardial cells," (2002).

[9]N. Sperelakis and J. E. Mann Jr, "Evaluation of electric field changes in the cleft between excitable cells," Journal of theoretical biology **64**, 71–96 (1977).

[10]N. Wei and E. G. Tolkacheva, "Mechanisms of arrhythmia termination during acute myocardial ischemia: Role of ephaptic coupling and complex geometry of border zone," PloS one **17**, e0264570 (2022).

[11] S. George, M. Bonakdar, M. Zeitz, R. Davalos, J. Smyth, and S. Poelzing, "Extracellular sodium dependence of the conduction velocity-calcium relationship: evidence of ephaptic self-attenuation," Biophysical Journal **110**, 30a–31a (2016).

[12] S. A. George, G. Hoeker, P. J. Calhoun, M. Entz, T. B. Raisch, D. R. King, M. Khan, C. Baker, R. G. Gourdie, J. W. Smyth, *et al.*, "Modulating cardiac conduction during metabolic ischemia with perfusate sodium and calcium in guinea pig hearts," American Journal of Physiology-Heart and Circulatory Physiology **316**, H849–H861 (2019).

[13] G. S. Hoeker, C. C. James, A. N. Tegge, R. G. Gourdie, J. W. Smyth, and S. Poelzing, "Attenuating loss of cardiac conduction during no-flow ischemia through changes in perfusate sodium and calcium," American Journal of Physiology-Heart and Circulatory Physiology **319**, H396–H409 (2020).

[14] R. Veeraraghavan, J. Lin, G. S. Hoeker, J. P. Keener, R. G. Gourdie, and S. Poelzing, "Sodium channels in the cx43 gap junction perinexus may constitute a cardiac ephapse: an experimental and modeling study," Pflügers Archiv-European Journal of Physiology **467**, 2093–2105 (2015).

[15] E. D. Copene and J. P. Keener, "Ephaptic coupling of cardiac cells through the junctional electric potential," Journal of mathematical biology **57**, 265–284 (2008).

[16] J. Lin and J. P. Keener, "Modeling electrical activity of myocardial cells incorporating the effects of ephaptic coupling," Proceedings of the National Academy of Sciences **107**, 20935–20940 (2010).

[17] J. Lin and J. P. Keener, "Ephaptic coupling in cardiac myocytes," IEEE Transactions on Biomedical Engineering **60**, 576–582 (2013).

[18] Y. Mori, G. I. Fishman, and C. S. Peskin, "Ephaptic conduction in a cardiac strand model with 3d electrodiffusion," Proceedings of the National Academy of Sciences **105**, 6463–6468 (2008).

[19] N. Wei and E. G. Tolkacheva, "Interplay between ephaptic coupling and complex geometry of border zone during acute myocardial ischemia: Effect on arrhythmogeneity," Chaos: An Interdisciplinary Journal of Nonlinear Science **30** (2020).

[20] N. Wei, Y. Mori, and E. G. Tolkacheva, "The dual effect of ephaptic coupling on cardiac conduction with heterogeneous expression of connexin 43," Journal of theoretical biology **397**, 103–114 (2016).

[21] K. Tsumoto, T. Ashihara, N. Naito, T. Shimamoto, A. Amano, Y. Kurata, and Y. Kurachi, "Specific decreasing of na+ channel expression on the lateral membrane of cardiomyocytes causes fatal arrhythmias in brugada syndrome," Scientific reports **10**, 19964 (2020).

[22] S. A. George, K. J. Sciuto, J. Lin, M. E. Salama, J. P. Keener, R. G. Gourdie, and S. Poelzing, "Extracellular sodium and potassium levels modulate cardiac conduction in mice heterozygous null for the connexin43 gene," Pflügers Archiv-European Journal of Physiology **467**, 2287–2297 (2015).

[23] J. P. Kucera, S. Rohr, and Y. Rudy, "Localization of sodium channels in intercalated disks modulates cardiac conduction," Circulation research **91**, 1176–1182 (2002).

[24] P. E. Hand and C. S. Peskin, "Homogenization of an electrophysiological model for a strand of cardiac myocytes with gap-junctional and electric-field coupling," Bulletin of mathematical biology **72**, 1408–1424 (2010).

[25] J. Lin and J. P. Keener, "Microdomain effects on transverse cardiac propagation," Biophysical journal **106**, 925–931 (2014).

[26] R. Veeraraghavan, S. Poelzing, and R. G. Gourdie, "Intercellular electrical communication in the heart: a new, active role for the intercalated disk," Cell communication & adhesion **21**, 161–167 (2014).

[27] J. B. Picone, N. Sperelakis, and J. E. Mann Jr, "Expanded model of the electric field hypothesis for propagation in cardiac muscle," Mathematical and computer modelling **15**, 17–35 (1991).

[28] L. M. Livshitz and Y. Rudy, "Regulation of ca2+ and electrical alternans in cardiac myocytes: role of camkii and repolarizing currents," American Journal of Physiology-Heart and Circulatory Physiology **292**, H2854–H2866 (2007).

[29] S. A. Cohen and L. K. Levitt, "Partial characterization of the rh1 sodium channel protein from rat heart using subtype-specific antibodies." Circulation Research **73**, 735–742 (1993).

[30] S. A. Cohen, "Immunocytochemical localization of rh1 sodium channel in adult rat heart atria and ventricle: presence in terminal intercalated disks," Circulation **94**, 3083–3086 (1996).

[31] S. K. Maier, R. E. Westenbroek, K. A. Schenkman, E. O. Feigl, T. Scheuer, and W. A. Catterall, "An unexpected role for brain-type sodium channels in coupling of cell surface depolarization to contraction in the heart," Proceedings of the National Academy of Sciences **99**, 4073–4078 (2002).

[32] T. Uchida, M. Yashima, M. Gotoh, Z. Qu, A. Garfinkel, J. N. Weiss, M. C. Fishbein, W. J. Mandel, P.-S. Chen, and H. S. Karagueuzian, "Mechanism of acceleration of functional reentry in the ventricle: effects of atp-sensitive potassium channel opener," Circulation **99**, 704–712 (1999).

[33] S. B. Knisley and B. C. Hill, "Optical recordings of the effect of electrical stimulation on action potential repolarization and the induction of reentry in two-dimensional perfused rabbit epicardium." Circulation **88**, 2402–2414 (1993).

[34] C. M. Ripplinger, A. V. Glukhov, M. W. Kay, B. J. Boukens, N. Chiamvimonvat, B. P. Delisle, L. Fabritz, T. J. Hund, B. C. Knollmann, N. Li, *et al.*, "Guidelines for assessment of cardiac electrophysiology and arrhythmias in small animals," American Journal of Physiology-Heart and Circulatory Physiology **323**, H1137–H1166 (2022).

[35] M. R. Rivaud, J. D. Bayer, M. Cluitmans, J. van der Waal, L. R. Bear, B. J. Boukens, C. Belterman, L. Gottlieb, F. Vaillant, E. Abell, *et al.*, "Critical repolarization gradients determine the induction of reentry-based torsades de pointes arrhythmia in models of long qt syndrome," Heart rhythm **18**, 278–287 (2021).

[36] J. F. Gomez, K. Cardona, L. Martinez, J. Saiz, and B. Trenor, "Electrophysiological and structural remodeling in heart failure modulate arrhythmogenesis. 2d simulation study," PloS one **9**, e103273 (2014).

[37] C. Bonometti, C. Hwang, D. Hough, J. J. Lee, M. C. Fishbein, H. S. Karagueuzian, and P.-S. Chen, "Interaction between strong electrical stimulation and reentrant wavefronts in canine ventricular fibrillation," Circulation research **77**, 407–416 (1995).

[38] M. Orini, A. J. Graham, N. T. Srinivasan, F. O. Campos, B. M. Hanson, A. Chow, R. J. Hunter, R. J. Schilling, M. Finlay, M. J. Earley, *et al.*, "Evaluation of the reentry vulnerability index to predict ventricular tachycardia circuits using high-density contact mapping," Heart rhythm **17**, 576–583 (2020).

[39] L. Azzolin, S. Schuler, O. Dössel, and A. Loewe, "A reproducible protocol to assess arrhythmia vulnerability in silico: pacing at the end of the effective refractory period," Frontiers in physiology **12**, 656411 (2021).

[40] R. A. Gray, A. M. Pertsov, and J. Jalife, "Incomplete reentry and epicardial breakthrough patterns during atrial fibrillation in the sheep heart," Circulation **94**, 2649–2661 (1996).